MAGIC: Magnetic Resonant Coupling for Intra-body Communication

Stella Banou, Kai Li, and Kaushik Chowdhury
Electrical and Computer Engineering Department, Northeastern University, Boston, MA, USA

***Abstract*—This paper proposes MAGIC: magnetic resonant (MR) coupling for intra-body communication between implants and wearables. MAGIC includes not only the hardware-software design of the coupled coils and methods of manipulating the magnetic field for relaying information, but also the ability to raise immediate emergency-related alerts with guaranteed delivery time. MR coupling makes the design of the transmission link robust to channel-related parameters, as the magnetic permeability of skin and muscle is close to that of air. Thus, changes in tissue moisture content and thickness does not impact the design, which is a persistent problem in other approaches for implant communications like RF, ultrasound and galvanic coupling (GC). The paper makes three main contributions: It develops the theory leading to the design of the information relaying coils in MAGIC. It proposes a systems-level design of a communication link that extends up to 50cm with a low expected BER of 10^{-4}. Finally, the paper includes an experimental setup demonstrating how MAGIC operates in air and muscle tissue, as well as a comparison with alternative implant communication technologies, such as classical radio frequency and GC. Results reveal that MAGIC offers instantaneous alerts with up to 5 times lower power consumption compared to other forms of communication.**

I. Introduction

Intra-body implants and wearables promise to revolutionize healthcare by early detection of life-threatening ailments, remote diagnosis by medical professionals, and real-time drug delivery [1]. While platform miniaturization and advances in implementing biochemical lab-on-a-chip have resulted in cm-scale sensing devices, how to interconnect them together for reliable and timely communication of the sensed data remains an open challenge. Although, wireless links that use classical microwave RF frequencies have been implemented in devices like heart pacemakers [2], RF is yet to see widespread adoption given associated risks of (i) tissue heating and (ii) extremely low energy efficiency that requires frequent recharging. Instead, we propose a different solution: 'MAGIC' that modulates data over magnetic resonant (MR) coupling, as opposed to classical electromagnetic RF radiation. Furthermore, we demonstrate in this paper that MAGIC has unique features that make it suitable for implant communication over other competing technologies, such as low sensitivity to water/salt content changes in the body tissue, ability to form long-distance links, and low power consumption.

A. Limitations of Current State-of-the-art

Safety and low energy consumption are primary drivers in selection of implant communication technology. While conventional narrow/ultra wide-band RF has seen practical deployment, RF signals experience high levels of signal attenuation in the body tissue, in the order of 60-80 dB [3] for distances of 15-20 cm, limiting the active lifetime of the implant. The transmission distance is also limited to ensure compliance with the limits introduced by the International Commission on Non-Ionizing Radiation Protection (ICNIRP) that defines permissible Specific Absorption Rate (SAR) and Maximum Permissible Exposure (MPE) to electromagnetic fields by tissue type [4].

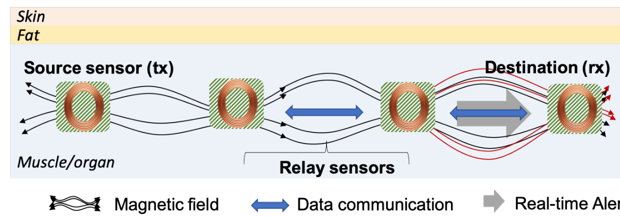

Fig. 1: An array of implanted sensors with near-field magnetic resonance coupling communication systems. MAGIC allows energy hopping via passive intermediate coils.

There are other non-traditional forms of intra body communication. *Ultrasound*, for example, uses acoustic waves well above the 20 kHz range. However, this technology is suitable for regions of the body that have greater water concentration (thus, not suitable for regions with bones). It also requires predictable knowledge of water concentration to accurately map transmission parameters to the channel conditions in the body. The different organs and tissues if varying sizes create a multipath environment that must be estimated via models and compensated for a successful ultrasound communication system design [5]. Additionally, ultrasound requires specialized nozzles and directional communication protocols that adds to both hardware and software complexity for an embedded implant. Alternatives like *Capacitive Coupling* enables the propagation of near electric fields around and throughout the human body, creating links that span the length of the medium [6]. However, both the transmitter and receiver need to share a common ground, which is not possible even for two implants physically separated within the same body. Thus, this technology is more promising for applications in touch-based authentication with external devices, instead of implant-implant communication [7]. Recent prototypes using techniques like *Galvanic Coupling* have shown many desirable properties of low-energy and simplicity of design by transmitting weak electrical currents of 0.5mA that is modulated with information bits. However, the channel model in this case is highly sensitive to the tissue thickness, hydration levels and positioning of electrodes [8].

B. MAGIC and Magnetic Resonant (MR) Coupling

In MR coupling, a source coil generates an oscillating magnetic field. This field induces electric current in the receiver coil, which further changes the voltage across a load resistor. By modulating the magnetic field with information, we establish a data channel. Compared to non-resonant cases, the receiver coil has carefully chosen inductive (L) and capacitive (C) elements to form a tuned LC circuit with a frequency of resonance given by Equation (1) [9]. If the transmitter coil modulates the magnetic field with the same frequency ω, it results in optimal power transfer, thereby also increasing the link distance (see Fig. 1).

$$\omega = \frac{1}{\sqrt{LC}} \tag{1}$$

MAGIC takes this concept of MR further by having a number of small resonating coils (each coil being part of an independent implant) forming a so called *energy relay*. In a completely passive manner, these intermediate coils help the source (say, the coil on the far left in Fig. 1) to extend its communication range beyond point-to-point links that is the defacto method to reach longer distances, irrespective of the choice of implant communication technology. Thus, the ability to create relays of coils opens up many new exciting directions for full body connected sensors, and research on routing and upper layer protocol design. This extension is not simplistic store-and-forward operation by the intermediate coils, but active shaping and strengthening of the magnetic flux density around the propagation path.

C. Additional Key Benefits in MAGIC

While extending the range of the data link has significant benefits, we would like to point out two additional software-defined control features in MAGIC that are critical in implant communication: Healthcare scenarios often require transmission of immediate alerts when anomalies are detected. CSMA/CA does not provide guarantees of time-bound packet delivery [10]. Time-slotted protocols may incur significant wait time in a multi-node environment [11]. MAGIC provides a framework enabling an intermediate node wanting to send an alert message to autonomously alter the magnetic field around itself - and through the coupling effect - at the destination as well. This is carefully done so that the ongoing transmissions from a regular reporting node is not interrupted, but the subtle variations introduced in the field is enough to convey to the destination the state and location of the alert.

Finally, the MR coupling in MAGIC fully addresses the issue of channel-dependent protocol changes required in Ultrasound and Galvanic Coupled communication. The magnetic field strength at the receiver coil depends on the magnetic permeability of the medium. The magnetic permeability of muscle tissue, as well as other human tissues, such as skin, is very close to that of air. This makes intra-body MR communication tissue independent, which helps to create a robust and standard protocol layer compared with other coupling methods.

The main contributions of our work are as follows:

1) We develop the theory of relay coils for miniaturized near-field MR communication using On-Off Keying (OOK).
2) We design a network of MR coil-equipped implant sensors that can transmit information over 10 cm distance between successive nodes. Our design includes the hardware and software development of the network, along with algorithms that reconfigure the electrical properties of resonating coils to transmit alert information.
3) We implement a testbed of 5 coil-enabled sensors to extend the end-to-end communication range to 50cm. We test our system embedded in muscle. We demonstrate experimentally the communication benefits using MR and evaluate the cost-benefits of the real-time alert transmission method. Additionally, we compare experimental results from MAGIC with other technologies like Galvanic Coupling and RF.

II. Related Work on Magnetic Coupling

A number of alternative intra-body communication methods with their cost-benefit trade-offs have been surveyed earlier in [6].For the purpose of this paper we focus our related work section on magnetic coupling methods.

Magnetic resonance coupling and inductive coupling are two similar magnetic coupling methods used primarily for wireless energy transfer with a focus on wireless charging. Magnetic resonance coupling occurs between two coils resonating in the same frequency when each connecting in series with a capacitor [12]. In [13], the properties of electromagnetic resonance are exploited to generate a magnetic field throughout the body. The authors propose near-field wireless transmission of electrical energy between two coils wrapped around parts of the body, driving the field propagation. The spectrum range most commonly used here extends from DC up to 50 MHz, yielding a maximum attenuation of only 8.1 dB, for a 40 cm distance covered [13]. We increase the coverage of MR communications by proposing MAGIC. In [13] there is no indication of the effect of the communication medium (air, human tissue) on the quality of communication. The wavelength of the magnetic field proposed in the work in [13] is 2.3m, which can potentially interfere with the magnetic fields of other nearby devices.

Magnetic coupling for wearables is simulated in [14] with promising results on transmission characteristics compared to other intra-body communication methods. Here, the magnetic field distribution around the arm is modeled to predict the effect of movement on communication. [15] makes a case for the robustness of magnetic inductance within non-magnetic environments through modeling and analysis. Thus, while there are some preliminary attempts at using magnetic coupling for wearable communications, there are no system implementations for both wearable and implantable scenarios. MAGIC provides a system design and implementation for not only communication between a source transmitter and destination, but a network of intermediate nodes, taking a stride towards full system implementation.

Similar to magnetic resonance coupling, inductive coupling transfers energy from one coil to another via a magnetic field. A commercial product that uses inductive coupling concept but for a completely different wireless charging application concerns powering smart-devices through the Qi-protocol [16]. Research on the use of magnetic inductance for communications shows promising results with low path-loss in environments such as underground or underwater [17], [18]. Unlike magnetic resonance coupling, inductive coupling requires perfect alignment and covers very small separation distances, in the order of millimeters [19].

Like Qi, the concept of relaying energy using intermediate resonating coils in MR has been explored earlier. The term "domino forms" is coined in [9] to describe the configuration of aligned coils resonating in the same frequency to transfer energy. Instead of using energy transfer for powering (charging), we use it for modulating data to communicate wirelessly. Thus, the purpose of energy-relay coils is different in MAGIC. These energy relays, previously demonstrated for large foot-long diameter coils, are engineered in a novel way in MAGIC with appropriate parameter settings to scale their size down to centimeters.

III. Communication with Energy Relaying Coils

In this section, we describe how the passive resonating coils are used for near-field intra-body communication used within MAGIC. Central to our approach is the theory of *energy hopping* across these coils, with each intermediate coil strengthening the magnetic field by suitable selection of its own impedance. Our objective here is to derive the expression for the induced electric current in the destination coil as a function of (i) the current in the source coil and (ii) the choice of suitable impedance values at the intermediate coils between them.

A. Theoretical framework for data communication

We now obtain the mathematical equations that give the induced current in the destination coil. Consider a linear array of equally-spaced coils that form a so called magnetic metamaterial at resonant coupling frequency, i.e., a virtual waveguide that aligns the magnetic field along the axis passing through the set of coupled coils. The circuit diagram for this coil arrangement is shown in Fig. 2. The left-most coil, as the source coil, modulates the magnetic field and transmits information to the far-right destination coil. L_n, C_n, and Z_n represent the inductance, capacitance, and complex impedance at the n-th coil, respectively. M_{nm} is the mutual inductance between nearest neighboring coils, where $n \neq m$ and n, m are integers.

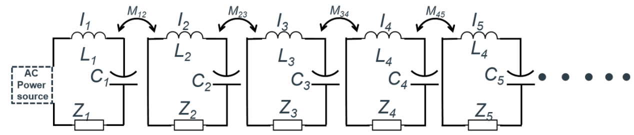

Fig. 2: Circuit diagram of an array of n coils with individual inductive and capacitive elements, and mutual coupling between them.

1) Source coil voltage-current relationship: An alternating voltage V_1 applied to the left-most coil, i.e., the source coil of the array, sets up a current I_1 given by,

$$V_1 = I_1(j\omega L_1 + \frac{1}{j\omega C_1} + Z_1) - j\omega M_{12} I_2 \tag{2}$$

where, L_1, C_1, and Z_1 represent the inductance, capacitance, and complex impedance at the transmitter. Similarly, I_2 is the current flowing through the second coil from the left. M_{12} is the mutual inductance of the transmitting source coil and its neighbor. Essentially, (2) relates a change in voltage on node 1 to its current (I_1), which in term affects the current of its neighboring coil (I_2) via changes in the induced magnetic field.

Magnetic flux density (B) is directly related to the magnetic field strength (H) by $B = \mu_r \mu_0 H$, where μ_r and μ_0 are the relative permeability and permeability of free space, respectively. Magnetic flux density is also related to current displacement by the Maxwell-Ampere equation and the Biot-Savart law. The Maxwell-Ampere law relates electric current with magnetic flux (b) in a wire or loop [20]. The Biot-Savart law relates the magnetic field contribution to its source current element [21]. For a looped wire forming a coil, such as n_1 in Fig. 2, the expression for the magnetic field tangent simplifies to:

$$B = \frac{\mu_0 I_1}{2R} \tag{3}$$

where R is the radius of the coil. Voltage is directly related to current if impedance remains the same. Therefore, (2) and (3) describe the relationship between magnetic flux density, magnetic field, voltage and current.

2) Intermediate-coil voltage-current relationship: Since the intermediate relay coils do not draw power actively, the sum of all currents that flow through any passive relay coil at resonant frequency defined by the choice of L-C combination (1) is zero. This is expressed formally in (4).

$$I_n(j\omega L_n + \frac{1}{j\omega C_n} + Z_n) + j\omega M_{n,n-1} I_{n-1} + j\omega M_{n,n+1} I_{n+1} = 0 \tag{4}$$

At resonance state, inductance $j\omega L_1$ and $\frac{1}{j\omega C_1}$ cancel each other out and therefore the impedance of coil n becomes equal to Z_n. We simplify this expression further to achieve a generic expression for the current induced in a neighboring coil. We assume equal distance between all coils to ensure their respective mutual coupling remains constant (i.e., $M = M_{nm}$) and set $X = j\omega M$.

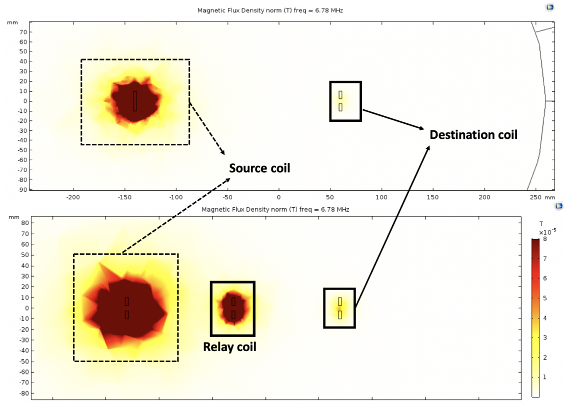

Fig. 3: COMSOL simulation of Magnetic Flux Density (B) with (bottom) and without (top) relay coil

3) Source current, destination current and data communication: To explain the induced current at the destination coil we use the concept of magnetoinductive waves (MIWs) from classical physics [22]. MIWs are formally defined as the propagation of magnetic energy in cells (here, nodes) that are coupled by mutual inductance (M). The current induced in one node stimulates current in the neighbouring nodes and this propagation creates MIWs.

The MIWs resulting from the combined action of the coil array sets up an induced current in the destination coil as follows: $I_n = I_0^{(-n\gamma d)}$, where I_0 is constant (the current through the source coil) and d is the distance of coil n to its nearest coil. The value of γ is defined as $\gamma = \alpha + jk$, where α is the attenuation coefficient that depends on the medium of communication and k is the wave number. Simplifying (4), the relationship between the currents of two neighboring coils in an infinite array is given by (5).

$$I_n(Z_n) + X(I_{n-1} + I_{n+1}) = 0 \tag{5}$$

We see the relationship between the induced current at the source (a function of voltage and coil impedance) and destination in (5). The current induced at the destination coil is proportional to the voltage applied to the source coil. In order to transmit data, varying the voltage at the source coil has an effect on the source current, the current at the intermediate nodes and the induced current at the receiver.

B. Visualization of energy relay coils

We conduct a COMSOL simulation of the magnetic field around a coil array to further study the effects of frequency and coil size on the performance of energy hopping. Fig. 3 shows three coils that are equidistantly placed in a muscle medium at 10 cm separation. We choose to simulate at 6.78 MHz, one of the commonly used frequencies for magnetic resonance wireless power transfer [23]. Each coil is a square of side 2 cm. The spatial extent of the magnetic flux density (B) defined deterministically through (3) is now simulated with and without the presence of a passive relay coil. The left-most source coil has the largest magnetic flux density due to the

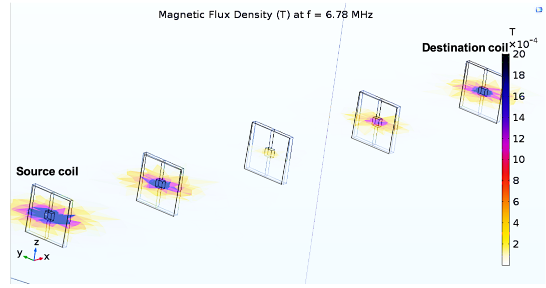

Fig. 4: 5-node network resonating at 6.78 MHz

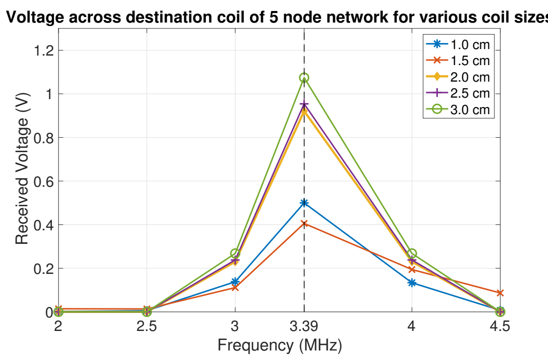

Fig. 5: The effect of coil size and capacitance to received voltage at the sink node. The chosen coil is circular of radius 2 cm.

transmission of a sinusoid signal. As a direct outcome of the analysis of the previous section, we see that the destination coil sees a higher magnetic flux density when the intermediate coil is present to strengthen the field, i.e., when the presence of the intermediate coil is analogous to a relay, shaping the energy towards the destination.

C. Resonance parameters: coil size and frequency

The parameters affecting the magnetic field strength - hence, the energy relay - are inductance, capacitance and frequency, related by Equation (1). As explained in [24], the bandwidth of information that can be modulated in this type of channel increases with the mutual inductance M between coils. For this reason, using identical coils with high mutual inductance is advisable. Attenuation of the signal occurs due to losses related to the self-inductance of coils. The inductance of the coil depends on its size and number of turns. We investigate the relationship of all the above by setting up a simulated energy relay coil system of resonating nodes. The COMSOL simulation setup includes 5 equidistant, identical coils at 10 cm apart (Fig.4). Each coil is connected in parallel with a capacitor which resonates at 3.39 MHz according to Resonance Equation (1). We choose the frequency used later for the system implementation. We notice that the coils resonating at a frequency of 3.39 and 6.78 MHz have the same behavior as long as they are tuned in according to (1). In Fig. 5 we see that all coil sizes give the highest received voltage at resonance (3.39 MHz). We also observe a relationship between coil size and the received voltage at resonance. Larger coil sizes lead to higher received voltage because the transmission distance of a coil is proportional to the coil size [9]. From this, the relationship between distance of communication and coil size is evident - smaller coil radius results in smaller communication distance. Thus, one of the design trade-offs we explore is how small can the coil dimensions be to better suit an implant use, while retaining its ability to communicate appreciable voltage changes.

IV. Communication System Design

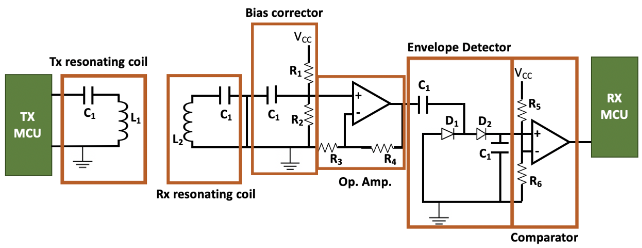

Fig. 6: Architecture of MR-coupled single-link transmitter and receiver

The theoretical analysis presented earlier allows us to study the impact of the coil dimensions, frequency of operation and modulation/demodulation circuit design of the nodes, while ensuring size and safety constraints are met for implant scenarios We next explain how we create a communication link between the source and destination: In the first stage, we set up a single link between two successive nodes, with careful attention to the hardware design. In the second stage, we develop a protocol for multiple nodes arranged in an array, capable of issuing an on-demand alert.

A. Hardware system design

Each node consists of a front-end with a resonating coil as the antenna (see Fig. 6), the transmitter and receiver electronics, and a micro-controller unit (MCU) to perform the software tasks of sensing and protocol execution. To transmit data, the source node MCU uses an OOK scheme. Each pulse consists of a sine wave at center frequency of 3.39 MHz. We select this value based on the self-inductance of the coils and the capabilities of the pin output of the MCU used for generating the OOK pulse signal. As mentioned in III-C, the frequencies 3.39 MHz and 6.78 MHz (used in magnetic resonance power transfer systems) have the same behavior, so we chose one without loss of generality. The data bits change the amplitude of the OOK square pulse as a digital ‘1’ for 3.3 V and ‘0’ for 0V at the Transmitter. The width of each pulse is 1 ms. At the destination, the MCU performs the decoding and demodulation tasks. The front-end electronics of the receiver chain are responsible for processing the signal to create a detectable square wave that can be read at the MCU. Inductors L_1 and L_2 are circular coils with diameter of 2 cm that resonate with capacitors C_1 and C_2, respectively.

TABLE I: Relative Permeability values

Medium	Relative permeability (μ_r)
Air	1.00 [25]
Water	0.99 [25]
Blood	1.0 [26]
Fat	1.44 [27]
Bone	1.78 [27]

TABLE II: Simulation results for communication medium

Medium	Source coil MFD (T)	Destination coil MFD (T)	Dest. Coil Current (mA)
Air	0.0052	0.0023	1.931
Muscle	0.0053	0.0025	2.000
Skin	0.0053	0.0025	2.001

B. Effect of communication medium to system design

We recall from Sec. III the effect of the relative permeability μ_r on the magnetic field and coil current. Since the primary application of MAGIC is for implanted and wearable nodes, how the communication medium impacts the channel between coils is an important design factor. The magnetic permeability of various human tissue types and air is summarized in Table I. As specific muscle and skin tissue permeability has not been measured or calculated before, due to the high levels of blood and water content, we assume their respective relative permeability values to be close to 1.0, as is common in magnetic coupling research [13], [15]. However, in order to investigate further the effect of the communication medium on the energy hopping between coils, we work with the simulation setup of Section III-C (Fig. 4) and change the material where the coils are placed in. COMSOL allows for the selection of materials from a large database. We measure the (i) current through the destination coil as well as (ii) the magnetic flux density at the source coil and destination coil while changing the medium to muscle, air and skin. We measure the magnetic flux density at the center of the respective coils.Our simulation results are summarized in Table II. As we see from the results, muscle, skin and air have the same effect on the magnetic flux density and induced current.

C. Choosing capacitors to make/break resonance

Error-free data reception depends on the amplitude of the voltage at the destination coil, which in turn depends on the induced current within it and that in the neighboring coils (2). Furthermore, the resonance condition resulting from the choice of the inductance and capacitance determine the current at resonance given in (1). Thus, when all coils are in resonance at the same frequency, the received voltage amplitude is maximized. Any change in capacitance along the chain of nodes immediately impacts the amplitude of the received voltage at the final node of the chain.

Both the communication system and alert generating mechanism by an intermediate node utilize intentionally set capacitor values to influence the receiver voltage. Each node has two capacitors connected to their coils: the default resonating capacitor C_{res} and a second capacitor denoted by C_{alert} with a value different than that of C_{res} given in (1). C_{alert} is chosen distinctly for each intermediate node and these values are

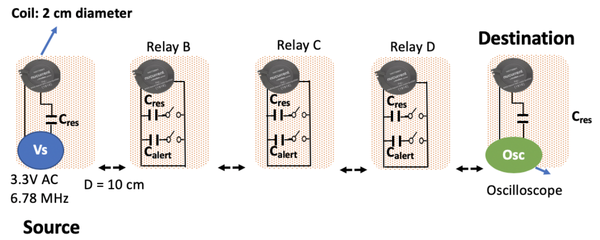

Fig. 7: Schematic of the testbed to demonstrate the alert concept using multiple capacitors connected to the coil array. Intermediate coils B/C/D can raise an alert at destination when source is concurrently transmitting.

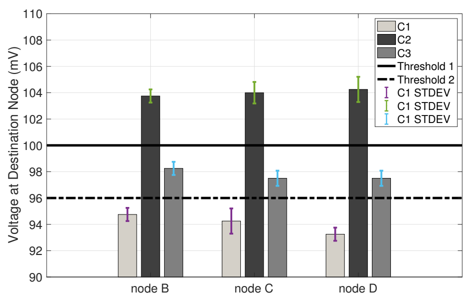

Fig. 8: Effect of the choice of capacitance on the received peak-to-peak voltage level at destination coil

embedded in each implant prior to deployment. We perform a preliminary study to investigate the change in the received voltage at the destination node, while switching from the resonating capacitor C_{res} to C_{alert} at each intermediate node. The setup consists of a five-node array, with the left-most node as the source and right-most node as destination (Fig. 7). The transmitting voltage is 3.3 V and the receiving voltage at resonance is 200 mV. The Tx voltage value was chosen based on typical output of battery sources used for low-power devices and wearables. The intermediate nodes (referred to as B, C and D for ease of explanation) are assigned C_{alert} values as $C_1 = 147pF$, $C_2 = 200pF$ and $C_3 = 780pF$. The results of 4 measurements per node and per C_{alert} value are presented in Fig. 8. From these initial results, we conclude that the different non-resonating values of C_{alert} lead to a distinct voltage change. The voltage level is not affected by which node switches to C_{alert} but by the value of C_{alert}. Therefore, the destination can immediately detect the location (i.e., node B, C or D) of the alert as soon as the corresponding intermediate node switches to its distinct C_{alert} value.

D. Protocol design

We explain the design of a simple link-PHY protocol in MAGIC for both data communication and the alert system. Consider a designated end point/destination node that serves as the data aggregator from all active implants. This destination node can be placed close to the skin or embedded in a wearable.

1) Node addressing and channel access: Each node has an ID that the destination node uses to select the order of

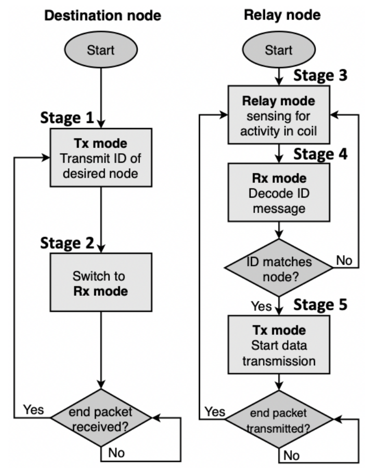

Fig. 9: Logic at implanted nodes

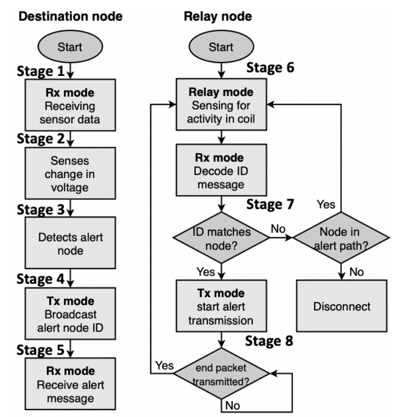

Fig. 10: System logic during alert situation

transmissions, as seen in Fig. 9. In order to conserve power, all nodes are in relay mode, i.e., a passive, idle mode where the MCU wakes up when activity is sensed on the coil. The destination node broadcasts the ID of the next transmitter (Stage 1 in Fig. 9). Any node that senses activity in its coil wakes up and decodes the ID (Stage 4). If the ID is not the node's, it goes back to relay mode. The result of this step is that only the TX node with the matching ID is active (due to Stage 5) and the rest of the nodes continue to remain in the low-power relay mode (Stage 3). For the actual transmission duration, the intermediate nodes stay in relay node and passively assist in energy hopping, as described in section III-A. Once data transmission from the selected transmitter is completed, the destination node broadcasts another ID for a new node to begin transmission.

2) Energy consumption: The active energy consuming nodes in MAGIC are the source transmitter and destination nodes during each transmission cycle. We estimate the energy consumption of the system based on((6)).

$$E_c = ((P_{Tx} + P_{out}) \cdot T_{on}) + n \cdot P_{idle} \cdot t_{idle} + (P_{Rx} \cdot R_{on}) \quad (6)$$

Here, the variables P_{Tx} and P_{Rx} represent the power consumption from the transmitter and receiver electronics. P_{out} is calculated based on the output voltage and current of the transmitting MCU. T_{on} and R_{on}, represent the time that the transmitter and receiver MCUs are on active state (TX mode or RX mode).t_{idle} refers to the time that the n intermediate nodes are in idle mode (Realy mode). Similarly, P_{idle} is the power consumed by the relay MCUs in idle state. During communication between the selected transmitter and the destination node, the two MCUs are in active mode whereas all the nodes in-between are in idle mode. Based on Fig. 6, the energy consuming components of each transmitter or receiver are the MCUs and the operational amplifiers at the receiver. We evaluate the energy consumption of MAGIC after implementation in section V.

3) Generating alerts: A key novelty is the alert generation in MAGIC, i.e., the ability of a node to immediately create a detectable change in the magnetic resonance communication ongoing within the network. Consider that the destination node is actively decoding the data signal signal that the selected source node is transmitting. If one of the other relay nodes in the network has an alert to send - that alert can be a critical "dangerous" measurement of the phenomenon that the sensor is monitoring - then by switching to its C_{alert} capacitor, the voltage across the coil of the destination node is immediately impacted (Stage 2 in Fig. 10). The destination node detects that change and momentarily switches to TX mode and broadcasts the ID of the alert node (Stages 3 and 4 in Fig. 10). All nodes between the alert node and the transmitting node switch off to prevent the transmitting message from reaching the destination and the alert node at the same time starts transmitting the data that raised the alert (Stage 8). This allows the destination node to then receive and decode the complete alert message (Stage 5). After the alert is processed, the network resumes its normal communication functionality.

The entire system design is implemented on a 5-node network and evaluated in the following section.

V. Systems implementation and Performance Evaluation

The experimental evaluation setup in MAGIC consists of arranging 5 coils in a linear array, each of 2 cm radius and separated by 10cm from each other (see Fig. 11a). The resonating capacitor is selected at 3.39 MHz frequency, as discussed in IV-A. Table IV provides summary of all the parameters of the testbed. Each coil arrangement is connected to a Teensy MCU, together forming an "implant". Thus, there are 5 such implants, with the right-most (destination) node executing the steps outline in Algorithm 9. Overall, MAGIC nodes transmit and receive information at 1 kbps with a BER of 10^{-4} over a distance of 50 cm.

We use this setup for the following studies: For the communication link, we evaluate the performance of the energy relay on BER, and demonstrate the superiority of the MR approach compared to alternatives like Ultra Wide Band Radio Frequency (RF-UWB) [28] and Galvanic Coupling (GC) [29]. We investigate the performance of our system in 3 set-ups with synthetic human tissue. In addition, we also study the response time of the alert mechanism.

TABLE III: MAGIC test-bed parameters

Coil Radius	2 cm (μ_r)
Coil Inductance	4.0 μH
Coil Weight	1.95 g
Inter-node distance	10 cm
Frequency	3.39 MHz
C_{res}	550 pF
Tx power	1.2 dBm

A. Impact on BER

We measure the BER for 4 different set-ups: (i) a single 50 cm link with no intermediate nodes, (ii) one node at 25 cm away from the TX and RX, (iii) 2 nodes and (iv) finally 3 nodes at equal distances from each other. We also vary the TX power to investigate the minimum output power that gives a satisfactory performance. Fig. 12 reveals that cases with less than 2 relay nodes in between the source and destination nodes does not allow correct decoding of information. With 2 or 3 intermediate nodes the performance of the system reaches the target BER of 10^{-4}. This occurs because the intermediate nodes perform the energy hopping to increase the SNR of the system. They allow for the magnetic field that carries the modulated signal to increase its magnetic flux density in further distances, as seen in Fig. 3. The increased magnetic flux density, and therefore magnetic field strength given by (3) leads to a higher current at the destination node's coil, which in turn increases voltage amplitude. We conclude that a TX power of 1.2 dBm is required to achieve a BER of 10^{-4}.

B. Comparison with existing IBC technologies

We compare MAGIC in terms of BER, end-to-end delay and power consumption with other intra-body communication techniques, such as GC and traditional RF with a TDMA protocol. For the comparison with GC, we refer to the system in [30], which uses a similar transceiver and synthetic tissue. We compare two RF systems - an RF-UWB transceiver [31] for power consumption and a simulated RF-TDMA network [32] for delay, due to the lack of prior work on a single system with both energy and delay information.

We evaluate the BER performance of a single link in various set-ups to study the effect of propagation medium on the system performance. We place the source and destination coils in phantom muscle tissue to investigate the performance of an implanted node (See Fig. 11b). We also setup a communication link from the muscle through the fat and skin layers, to a node attached outside on the body to emulate a "wearable" setting (See Fig. 11c). Table IV includes the BER and propagation latencies of a single-hop communication for the above implanted scenarios as well as for the baseline case of over the air. The distance is constant at 10 cm in all three cases. The resulting average BER and delay values are statistically identical. This proves that MAGIC performs as predicted in wearable, implanted or over-the-air near-field setups and is robust to the presence of the specific channel. As compared

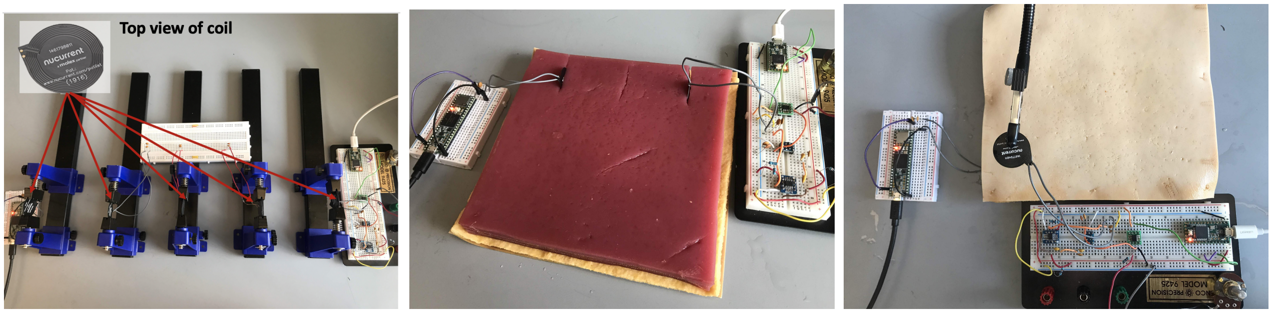

(a) over the air, 5 nodes- top view (b) synthetic muscle tissue (c) muscle, fat and skin - top view

Fig. 11: MAGIC implementation, over the air (a), single link (10 cm) implanted in muscle (b) and muscle to skin communication (c) (not pictured - source coil under phantom)

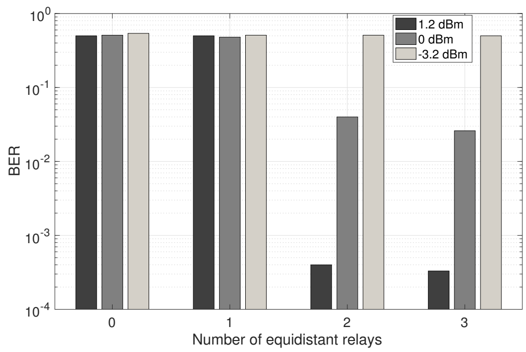

Fig. 12: BER at receiver over 50 cm with 0, 1, 2 or 3 equidistant passive relays placed in between Tx and Rx

TABLE IV: Single-hop performance metrics for 3 implementation scenarios

	Average BER	Average Delay (ms)
Over the air	4.0 E-4	3021
Implanted in muscle	2.9 E-4	3032
Muscle with fat, skin	4.0 E-4	3024

to this, previous work on GC exhibit up to 3 dB change in attenuation when the same tissue is used but at different measurement times, owing to changes in moisture content and salinity [8]. For RF intra-body systems, the propagation of the signal varies by tissue layer, therefore the placement of the sensors changes the behavior of the single link [33].

We obtain the energy consumption of the entire network of 3 and 5 nodes based on the current drawn by the Teensy MCUs at each mode (idle, Rx, Tx) and (6) for a 10% duty cycle of (transmitter and receiver are on for 10% of the time, relays always in idle mode). For MAGIC, we observe 586 mJ consumption for a 3-node network and 630 mJ for a 5-node network. The power consumption of each component is measured by connecting each node to a load resistor and obtaining the current across it. The voltage applied to both Tx and Rx is 3.3 V.

Energy savings is a key benefit when using MR coupling with energy relay coils to construct a near-field intra-body network. As the intermediate relay coils are passive, the size of the network in terms of number of intermediate hops does not cause an appreciable increase in the power consumption. We compare the power consumption for the 3-node and 5-node configurations in MAGIC with alternate methods like RF-UWB and GC in Fig. 13. In order to perform a fair comparison of power consumption, we only take into consideration the communication circuit power consumption and exclude the MCU power overhead that forms the rest of the implant. Thus, by comparing only the front-end electronics power consumption, we ensure that only the method of communication is evaluated instead of other benefits obtained by device engineering and miniaturization. We notice the rapid increase in power consumption between the 3-node and 5-node networks in the case of RF-UWB and GC, as opposed to the near-constant power consumption in MAGIC. The existence of the energy relay nodes leads to an increase in SNR across the network without the need for re-transmissions or an amplifier at the transmitter. This keeps the power consumption of MAGIC around 1.47 mW.

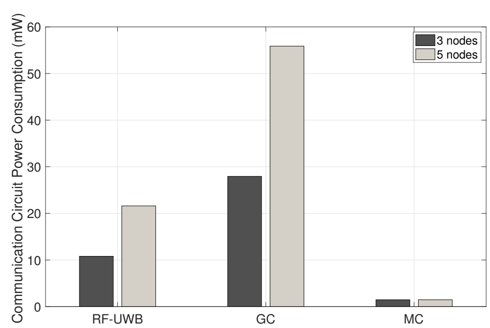

Fig. 13: Power consumption of 3-node and 5-node networks. Radio Frequency - Ultra Wide Band, Galvanic Coupling and MAGIC

We define *end-to-end delay* as the time elapsed from the start of transmission of the packet to its reception at the destination, after passing through the network. We measure this delay for 3- and 5-node in MAGIC, and compare it with previously published delay values for an RF network with TDMA [32] as well as GC (see Fig. 14). MAGIC maintains the delay of 3s for both network length (theoretically, same situation should occur for many more intermediate nodes). This is because the intermediate relay nodes do not alternate between receive and transmit modes during packet forwarding; instead they passively strengthen the signal (magnetic field variations) towards the destination. We notice that RF-TDMA has a lower delay of less than 2s for its worst case. This improvement over MAGIC is due to the larger bandwidth and packet rate adaptation algorithms in the RF communication method.

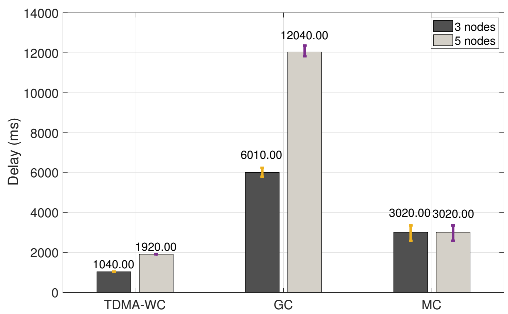

Fig. 14: End-to-end delay of 3-node and 5-node networks. Radio Frequency with TDMA (best and worse case scenario), Galvanic Coupling and Magnetic Resonance Coupling

C. Alert system evaluation

We implement a mode-selector switch at each relay node that connects the coil to a specific capacitor value. We measure the response time of MAGIC starting from the switching from the regular energy-relay mode of operation to an alert case, i.e., we measure the time between selecting the C_{alert} at the node desiring to notify the destination to the time taken by the latter to detect this change. The purpose of this measurement is to validate the claim that MAGIC allows detection of near-immediate alerts by the intermediate nodes.

We measure the voltage drop to 20 mV which is well within the detectable resolution of the destination coil MCU (Fig. 15). The voltage drop happens once we the connect the C_{alert} and disconnect the resonating capacitor by use of a switch. The voltage across C_{alert} increases rapidly. We observe that the detection of voltage drop at the destination happens instantaneously with the switch to C_{alert}. Then, from Algorithm 10, the destination initiates the transmission and reception of the alert message. In the case of a pure link-layer protocol TDMA, the time between issuing an alert by a node and the notification of the destination is limited by the time-slot duration. In the case of GC, for the same scenario the alert notification time is limited by the delay of one transmission. This delay, as seen in Fig. 14, can be several seconds. Thus, MAGIC provides an instantaneous alert notification independent of the network size, which is not possible in alternate methods.

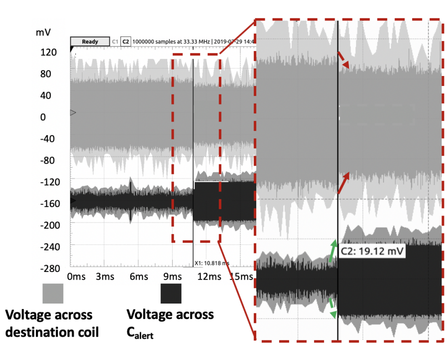

Fig. 15: Voltage measurement at destination coil (top) and across C_{alert} at relay node (bottom). At 10.818 ms the relay node switches from C_{res} to C_{alert}

.

D. Tissue safety in MAGIC

The MPE threshold for MR systems is 2.02 mW/cm^2 [6]. Consider a 5-node array in MAGIC, with the rest of the system design shown in Fig. 6. We measure the electric field in a 60x50x10 cm^3 volume of muscle tissue through a simulation study conducted in COMSOL. The simulation environment is setup as described earlier in the work on preliminary studies (see Sec. IV-C) (Fig. 4). We apply TX power of 1.2 dBm at the source coil while the 3 relay coils and the destination coil resonate at 3.39 MHz. We measure the electric field at a slice of the volume that transverses the center of the aligned coils. The electric field averages $3.81x10^{-6}mW/cm^2$ across the slice. Although the field strength is higher around the source coil, it does not exceed $4.12x10^{-3}mW/cm^2$, which is below the MPE mentioned above. This study verifies the safe design of MAGIC implants. Additionally, we measure the temperature increase of the muscle tissue surrounding the nodes in the same simulation. There is no appreciable rise, proving that there is no risky temperature related impact inside the body.

VI. Discussion and Conclusion

This paper develops the theory and presents the implementation of MAGIC, a framework for MR-based coupling for wearable and implantable sensor communication. We derive the theoretical expressions for energy hopping across an array of coils by inter-relating the voltage, current and the generated magnetic field. We design a network of nodes using an array of coils resonating in the same frequency, which performs communication of sensor data through OOK modulation. MAGIC shows how changing the amplitude of the voltage in the transmitter allows detecting those changes at the destination five hops and 50 cm away. An immediate alert notification setting is implemented on relay nodes by switching to a non-resonating capacitance. When compared with RF and GC, MAGIC provides faster alerts at a lower network power consumption.

In our next steps, we will develop a full protocol stack with medium access and error detection/recovery via hybrid FEC/ARQ settings. We will identify suitable modulation schemes (beyond OOK) that further improve data rate and optimize power consumption. Finally, we are working on studying the effect of miniaturization (moving coil dimensions from cm-scale to mm-scale).

Acknowledgment

This material is based on the work supported by the U.S. National Science Foundation under Grant No. CNS-1740907.

References

[1] T. T. Ruckh and H. A. Clark, "Implantable nanosensors: toward continuous physiologic monitoring," Feb 2014. [Online]. Available: https://www.ncbi.nlm.nih.gov/pmc/articles/PMC4106471/

[2] "New pacemaker technologies," Feb 2018. [Online]. Available: https://www.dicardiology.com/article/new-pacemaker-technologies

[3] V. D. Santis and M. Feliziani, "Intra-body channel characterization of medical implant devices," in *10th International Symposium on Electromagnetic Compatibility*, Sept 2011, pp. 816–819.

[4] I. C. on Non-ionizing Radiation Protection (ICNIRP), "Guidelines for limiting exposure to time-varying electric, magnetic and electromagnetic fields." [Online]. Available: https://www.icnirp.org/cms/upload/publications/ICNIRPemfgdl.pdf

[5] G. E. Santagati and T. Melodia, "Sonar inside your body: Prototyping ultrasonic intra-body sensor networks," in *IEEE INFOCOM 2014 - IEEE Conference on Computer Communications*, April 2014, pp. 2679–2687.

[6] W. J. Tomlinson, S. Banou, C. Yu, M. Stojanovic, and K. R. Chowdhury, "Comprehensive survey of galvanic coupling and alternative intra-body communication technologies," *IEEE Communications Surveys Tutorials*, pp. 1–1, 2018.

[7] H. Truong, P. Nguyen, V. Nguyen, M. Ibrahim, R. Howard, M. Gruteser, and T. Vu, "Through-body capacitive touch communication," in *Proceedings of the 9th ACM Workshop on Wireless of the Students, by the Students, and for the Students*, ser. S3 '17. New York, NY, USA: ACM, 2017, pp. 7–9. [Online]. Available: http://doi.acm.org/10.1145/3131348.3131351

[8] M. Swaminathan, F. S. Cabrera, J. S. Pujol, U. Muncuk, G. Schirner, and K. R. Chowdhury, "Multi-path model and sensitivity analysis for galvanic coupled intra-body communication through layered tissue," *IEEE Transactions on Biomedical Circuits and Systems*, vol. 10, no. 2, pp. 339–351, April 2016.

[9] W. Zhong, C. K. Lee, and S. Y. R. Hui, "General analysis on the use of tesla's resonators in domino forms for wireless power transfer," *IEEE Transactions on Industrial Electronics*, vol. 60, no. 1, pp. 261–270, Jan 2013.

[10] B. A. Forouzan, F. Mosharraf, B. A. Forouzan, and B. A. Forouzan, *Computer networks: a top-down approach*. McGraw-Hill, 2012.

[11] S. R. Ahamed, "Review and implications of time division multiple access techniques for wireless environment services and applications," *Journal of Theoretical and Applied Information Technology*.

[12] A. Karalis, J. Joannopoulos, and M. Soljacic, "Efficient wireless non-radiative mid-range energy transfer," *Annals of Physics*, vol. 323, no. 1, pp. 34 – 48, 2008, january Special Issue 2008. [Online]. Available: http://www.sciencedirect.com/science/article/pii/S0003491607000619

[13] J. Park and P. P. Mercier, "Magnetic human body communication," in *2015 37th Annual International Conference of the IEEE Engineering in Medicine and Biology Society (EMBC)*, Aug 2015, pp. 1841–1844.

[14] F. Koshiji, Y. Fujita, and K. Koshiji, "Wireless body area network using magnetically-coupled wearable coils," in *2015 IEEE CPMT Symposium Japan (ICSJ)*, Nov 2015, pp. 208–211.

[15] N. Golestani and M. Moghaddam, "Theoretical modeling and analysis of magnetic induction communication in wireless body area networks (wbans)," *IEEE Journal of Electromagnetics, RF and Microwaves in Medicine and Biology*, vol. 2, no. 1, pp. 48–55, March 2018.

[16] "Qi: Charging, simplified." [Online]. Available: https://www.wirelesspowerconsortium.com/about/benefits.html

[17] H. Guo, Z. Sun, and C. Zhou, "Practical design and implementation of metamaterial-enhanced magnetic induction communication," *IEEE Access*, vol. 5, pp. 17 213–17 229, 2017.

[18] Z. Li and Z. Sun, "Antenna system optimization for active metamaterial-enhanced magnetic induction communications," in *2019 13th European Conference on Antennas and Propagation (EuCAP)*, March 2019, pp. 1–5.

[19] C. Yang and C. Yang, "Analysis of inductive coupling coils for extending distances of efficient wireless power transmission," in *2013 IEEE MTT-S International Microwave Workshop Series on RF and Wireless Technologies for Biomedical and Healthcare Applications (IMWS-BIO)*, Dec 2013, pp. 1–3.

[20] "Gauss' law for electricity." [Online]. Available: http://hyperphysics.phy-astr.gsu.edu/hbase/electric/maxeq2.html

[21] "Biot-savart law." [Online]. Available: http://hyperphysics.phy-astr.gsu.edu/hbase/magnetic/Biosav.html

[22] E. Shamonina, V. A. Kalinin, K. H. Ringhofer, and L. Solymar, "Magnetoinductive waves in one, two, and three dimensions," *Journal of Applied Physics*, vol. 92, no. 10, pp. 6252–6261, 2002.

[23] T. Wang, T. Chu, and H. Lee, "Wireless power transfer with 6.78-mhz operation frequency on biological media (pork muscle)," in *2016 IEEE International Symposium on Radio-Frequency Integration Technology (RFIT)*, Aug 2016, pp. 1–3.

[24] C. J. Stevens, "Magnetoinductive waves and wireless power transfer," *IEEE Transactions on Power Electronics*, vol. 30, no. 11, pp. 6182–6190, Nov 2015.

[25] "Permeability." [Online]. Available: www.engineeringtoolbox.com/permeability-d1923.html

[26] "Broadband dielectric spectroscopy on human blood," *Biochimica et Biophysica Acta (BBA) - General Subjects*, vol. 1810, no. 8, pp. 727–740, 2011.

[27] G. Shimonov, A. Koren, G. Sivek, and E. Socher, "Electromagnetic property characterization of biological tissues at d-band," *IEEE Transactions on Terahertz Science and Technology*, vol. 8, no. 2, pp. 155–160, March 2018.

[28] S. A. Mirbozorgi, H. Bahrami, M. Sawan, L. Rusch, and B. Gosselin, "A full-duplex wireless integrated transceiver for implant-to-air data communications," in *2015 IEEE Custom Integrated Circuits Conference (CICC)*, Sep. 2015, pp. 1–4.

[29] W. J. Tomlinson, K. R. Chowdhury, and C. Yu, "Galvanic coupling intra-body communication link for real-time channel assessment," in *2016 IEEE Conference on Computer Communications Workshops (INFOCOM WKSHPS)*, April 2016, pp. 968–969.

[30] W. J. Tomlinson, S. Banou, S. Blechinger-Slocum, C. Yu, and K. R. Chowdhury, "Body-guided galvanic coupling communication for secure biometric data," *IEEE Transactions on Wireless Communications*, vol. 18, no. 8, pp. 4143–4156, Aug 2019.

[31] M. Ali, M. Sawan, H. Shawkey, and A. Zekry, "Fm-uwb transmitter for wireless body area networks: Implementation and simulation," in *2016 IEEE International Symposium on Circuits and Systems (ISCAS)*, May 2016, pp. 2395–2398.

[32] Q. Wang, K. Jaffres-Runser, Y. Xu, J.-L. Scharbarg, Z. An, and C. Fraboul, "Tdma versus csma/ca for wireless multihop communications: A stochastic worst-case delay analysis," *IEEE Transactions on Industrial Informatics*, vol. 13, no. 2, 2017.

[33] I. Dove, "Analysis of radio propagation inside the human body for in-body localization purposes," 2014.